

Improvement of interaction between pre-dispersed multi-walled carbon nanotubes and unsaturated polyester resin

M. D. H. Beg · A. K. M. Moshiul Alam ·
R. M. Yunus · M. F. Mina

Received: 31 July 2014 / Accepted: 23 December 2014 / Published online: 22 January 2015
© Springer Science+Business Media Dordrecht 2015

Abstract Efforts are being given to the development of well-dispersed nanoparticle-reinforced polymer nanocomposites in order to tailor the material properties. In this perspective, well dispersion of multi-walled carbon nanotubes (MWCNTs) in unsaturated polyester resin (UPR) was prepared using pre-dispersed MWCNTs in tetrahydrofuran solvent with ultrasonication method. Then the well-dispersed MWCNTs reinforced UPR nanocomposites were fabricated through solvent evaporation. Fourier-transform infrared spectroscopy indicates a good interaction between matrix and MWCNTs. This along with homogeneous dispersion of nanotubes in matrix has been confirmed by the field emission scanning electron microscopy. At low shear rate, the value of viscosity of UPR is 8,593 mPa s and that of pre-dispersed MWCNT–UPR suspension is 43,491 mPa s, showing implicitly a good dispersion of nanotubes. A notable

improvement in the crystallinity of UPR from 14 to 21 % after MWCNTs inclusion was observed by X-ray diffractometry. The mechanical properties, such as tensile strength, tensile modulus, impact strength, and elongation-at-break, of nanocomposite were found to be increased to 22, 20, 28, and 87 %, respectively. The estimated melting enthalpy per gram for composites as analyzed by differential scanning calorimetry is higher than that of UPR. The onset temperature of thermal decomposition in the nanocomposites as monitored by thermogravimetric analysis is found higher than that of UPR. Correlations among MWCNTs dispersion, nucleation, fracture morphology, and various properties were measured and reported.

Keywords Multiwall carbon nanotubes · Pre-dispersion · Polyester resin · Solvent evaporation · Reinforced polymer nanocomposites

M. D. H. Beg (✉) · A. K. M. Moshiul Alam (✉) ·
R. M. Yunus
Faculty of Chemical and Natural Resources Engineering,
Universiti Malaysia Pahang, Gambang, 26300 Kuantan,
Malaysia
e-mail: dhhbeg@yahoo.com

A. K. M. Moshiul Alam
e-mail: akmmalam@gmail.com

M. F. Mina
Department of Physics, Bangladesh University of
Engineering and Technology, Dhaka 1000, Bangladesh

Introduction

Unsaturated polyester resins (UPRs) are extensively used thermosetting resins that have received gradually increasing application in various sectors. Usually, liquid UPRs are solidified with crosslinking process because molecules of polymers or resins are joined together by curing process that not only raises the molecular weight of the polymers but also enhances their mechanical properties and thermal stability

(Pavlidoua and Papaspyrides 2008; Monti et al. 2011; Moshui Alam et al. 2012). Based on the types of polymers, different kinds of crosslinking processes are carried out. For instance, crosslinking of polymers can be done by means of different chemicals, heat, pressure, and ionizing radiations, such as electron beam, gamma or X-rays (Kubota 1975; Alam et al. 2011; Shubhra and Alam 2011; Mina et al. 2013). In all these cases, the structure of polymer is altered through chemical reactions. The curing of UPR is a free-radical copolymerization of the polyester and styrene molecules. The stimulation of free radicals in UPR occurs by either heat or the presence of a catalyst, thereby transforming resin from liquid state to cross-linked solid state through exothermic reactions (Kosar and Gomzi 2010). The curing is an important process, because it can improve mechanical properties and resistance to scratch, heat, chemicals, etc. of the cured products (Shubhra et al. 2011). However, cross-linked UPRs have limited structural reliability, and hence prior to crosslinking reaction, they are often mixed with reinforcing materials such as natural fibers, synthetic fibers, nanofillers, mineral fillers, and others in order to fabricate reinforced composites, which are being employed in construction, marine, and automotive industries due to their light weight and durability (Albdiry and Yousif 2013). Successful use of particulate-reinforced thermoset polyester resin composites (PCs) has enabled new combinations of mechanical, electrical, magnetic, optical, chemical, and surface properties. As a result, they find wide applicability in the automotive, aerospace, packaging, electronics, information, pharmaceuticals, biomedical, energy, sports goods, and personal care sectors, where the PCs are being used as self-regulating heating elements, current switching, fluid sensor, thermal controller, capacitors, electromagnetic interference shielding, radio frequency interference shielding, and electrostatic dissipation of charges (Genhua et al. 2004; Monti et al. 2011; Zhang et al. 2011; Gojny et al. 2005).

On the other hand, owing to their outstanding mechanical and electrical properties, low mass density, and high aspect ratio, carbon nanotubes (CNTs) have become more attractive substitutes than conventional macro- and micro-scaled fillers in the vicinity of polymer composites (Kayatin and Davis

2009). They are geometrically distinctive due to their surface structure and area, providing immense resources of interaction with any continuous phase and giving rise to a great opportunity to effective load transfer (Gojny et al. 2004). Besides, a small amount of CNTs with efficient dispersion in polymer matrix exhibits abundant enhancement of different properties (Kota et al. 2007). Any significant improvement in composite properties is determined by the degree of CNTs dispersion, interfacial adhesion of CNTs with the polymer matrix, and dispersed phase of the composite system (Singh et al. 2013). Conversely, several phenomena limit promising application of CNTs in composite technology. Of these, nanotube morphology and Van der Waal's forces between nanotube surfaces restrict homogeneous dispersion of CNTs in polymer matrix. The high aspect ratio together with the high flexibilities of CNTs noticeably increases the possibilities of their entanglements, and the entangled aggregates are very complicated to separate into individual nanotube (Breton et al. 2004). The Van der Waal's interaction among single-walled CNTs (SWCNTs) or multi-walled CNTs (MWCNTs) naturally makes them difficult to be separated into individual nanotube (Sun et al. 2005; Li et al. 2014). Therefore, different physical and chemical methods are established for controlling the dispersion of nanotubes in polymer matrix.

Physical method, like ultrasonication, involves direct mixing of CNTs using a mechanical force through application of ultrasound energy. Usually, it is done in an ultrasonic bath and has adjustable amplitude and power. However, if the sonication action is too violent and too long, CNTs surfaces can be severely damaged and nanotubes become amorphous carbon nanofibers (Lu et al. 1996; Mukhopadhyay et al. 2002). It has been reported that 1 h sonication has improved MWCNTs dispersion in epoxy matrix, thus enhancing thermo-mechanical properties of composite (Gkikas et al. 2012). This idea has also been considered in the present research in order to prevent MWCNTs from damage. Besides, chemical methods are carried out by action of surfactants, functionalization of carbon nanotube, surface modification, and polymer wrapping technology (Barber et al. 2003; Kim et al. 2012). Studies related to thermoset

nanocomposite systems have shown shear mixing strategies for dispersion of CNTs. These have been carried out at room temperature with different non-hydrogen bonding Lewis base solvents to take away the nanotube surface interaction (Ausman et al. 2000).

Among various CNTs, multi-walled carbon nanotubes (MWCNTs) are often incorporated with varieties of polymers as important reinforcements to obtain superior properties of the resulting materials, as driven by their unique thermal and electrical conductivities and robust mechanical modulus (Logakis et al. 2011; Hemmati et al. 2008; Ritter et al. 2010; Mina et al. 2010, 2014). It is expected that UPRs can have widespread application as compared to other resins, if their properties can be enforced by homogeneously dispersed MWCNTs. However, there have only been limited investigations on MWCNT-reinforced UPR composites (Battisti et al. 2009; Seyhan et al. 2007), where the authors claimed a good dispersion of nanotubes required to obtain a considerable increase in material properties. There still poses open questions about the homogeneous dispersion of MWCNTs in UPR-based composites. Consequently, this work has been undertaken to improve the dispersion of MWCNTs in UPR matrix by means of THF solvent and suitable sonication. In this article, the effect of MWCNTs dispersion on structural, surface morphological, and thermo-mechanical properties of the resulting nanocomposites as influenced by both THF solvent and sonication has been reported.

Materials and methods

Materials

Orthophthalic unsaturated polyester resin (Polymal) was used as received from Luxchem Polymer Industries Sdn. Bhd., Malaysia. The viscosity of resin is 700–800 mPa s at 25 °C. Its volatile content is 30–35 %, and gel time is 8–15 min. Multi-walled carbon nanotubes (MWCNTs), produced by moving-bed catalysis technique having diameter <8 nm, length between 10 and 30 µm, and carbon purity of 95 %, were collected from Timesnano, China. Tetrahydrofuran (THF) was purchased from Merk, Germany, and methyl ethyl ketone peroxide (MEKP) was procured from Sigma Aldrich, USA.

Methods

Composite fabrication

About 0.5 wt% of MWCNTs were mixed in THF solvent, maintaining the MWCNTs:THF ratio as 1:25. This suspension was mechanically stirred by a magnetic stirrer for 15 min, followed by the sonication in an ultrasound bath for 1 h. After that, it was mixed with resin and stirred again for 15 min and subsequently sonicated for 2 h. The resin/MWCNTs suspension was heated at the boiling temperature of THF (66 °C) for 5 min. The warm suspension was placed in a cold water bath to cool it at room temperature. MEKP (1 wt%) was added to this suspension as initiator for crosslinking and gently stirred for 3 min and then placed in vacuum to remove the bubbles. Finally, the bubble-free mixture was poured on the specimen mold and cured at room temperature. The nanocomposite of MWCNT and UPR was also prepared by the same technique as mentioned above without using THF. Thus, the prepared samples subjected to various measurements were neat unsaturated polyester resin (UPR), MWCNT-reinforced UPR nanocomposite (MWCNT–UPR), and THF solvent-dispersed MWCNT-reinforced UPR nanocomposite (THF–MWCNT–UPR).

Characterization

Viscosity

Viscosity measurement was conducted according to ASTM D2983 by the Brookfield DV-III ULTRA, rotary viscometer. In this case, the sample holder contained 9 ml of sample, while the container was maintained in a water-jacketed block at room temperature. The cylindrical spindle-31 is then rotated with different rpm ranges from 0.1 to 5.9, showing an individual share rate for each rpm, and the viscosity corresponding to share rate has been recorded in the unit of mPa s.

X-ray diffractometry

X-ray diffraction (XRD) data were collected using a Rigaku Mini Flex II, Japan, operated at 30 kV, at 15 mA and equipped with computer software to

analyze the data. The specimens were step-wise scanned over the operational range of scattering angle (2θ) between 3 and 40° , with a step of 0.02° , using Cu K_α radiation of wavelength $\lambda = 1.541 \text{ \AA}$. The data were recorded in terms of the diffracted X-ray intensities (I) versus 2θ . The degree of crystallinity (χ_c) was calculated using Eq. 1 (Wen Ling Zhang et al. 2011):

$$\chi_c = \frac{I_{cr}}{I_{cr} + I_{am}} \times 100, \quad (1)$$

where I_{cr} and I_{am} are the integrated intensities of crystal and amorphous parts of the samples, respectively.

Fourier transformation infrared spectroscopy

Fourier-transform infrared (FTIR) spectroscopy was carried out to detect the bonding natures in the composites. The measurements were conducted by a Nicolet 6700 FTIR spectrometer, Thermo Scientific, Germany using the standard KBr pellet technique in the wave number range of $4,000\text{--}500 \text{ cm}^{-1}$.

Field emission scanning electron microscopy

Composites' non-fractured and fractured surfaces were observed using a (JOEL, JSM-7800F, Japan) field emission scanning electron microscope. Samples were mounted on aluminum stubs with a carbon tape followed by a sputter coating with platinum to make them conductive prior to the field emission scanning electron microscopy (FESEM).

Tensile testing of composites

Tensile testing was conducted according to ASTM 638-08, using a Shimadzu (Model: AG-1) Universal tensile testing machine fitted with a 5 kN load cell and operated at a cross-head speed of 1 mm/min by keeping 65 mm gage length. Five samples of each category were tested for tensile strength (TS), tensile modulus (TM), and percentage of elongation-at-break (EB) measurements.

Impact testing

The impact test was carried out according to the EN ISO 179 by a Ray-Ran Pendulum Charpy Impact

System. The impact velocity was 3.5 m/s with the hammer weight of 0.163 kg. Dimensions of the samples were $80 \text{ mm} \times 8 \text{ mm} \times 3.5 \text{ mm}$; five replicates were evaluated for each type of samples to obtain impact strength (IS).

Differential scanning calorimetry

Differential scanning calorimetry (DSC) was performed to determine the thermal transitions in the material, using a TA/Q1000 apparatus under nitrogen atmosphere and ramp method. During DSC analysis, the samples were heated at temperatures in the range of $30\text{--}400 \text{ }^\circ\text{C}$ with a heating rate of $10 \text{ }^\circ\text{C min}^{-1}$.

Thermogravimetric analysis

Thermogravimetric analysis (TGA) was performed by a TGA Q500 V6.4, Germany in a platinum crucible under 60 % air and 40 % nitrogen atmosphere with a heating rate of $10 \text{ }^\circ\text{C/min}$. The temperature range was scanned from 20 to $700 \text{ }^\circ\text{C}$.

Result and discussion

Viscosity

Figure 1 shows a plot of viscosity as a function of shear rate for the suspensions of UPR, MWCNT-UPR, and THF-MWCNT-UPR. Apparently, the viscosity of the UPR is less dependent on the shear rate, whereas it changes like a complex fluid for

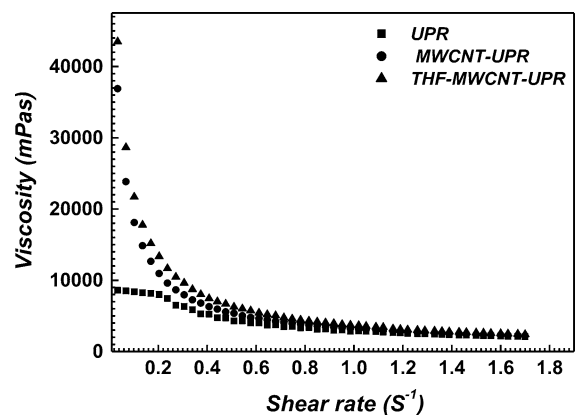
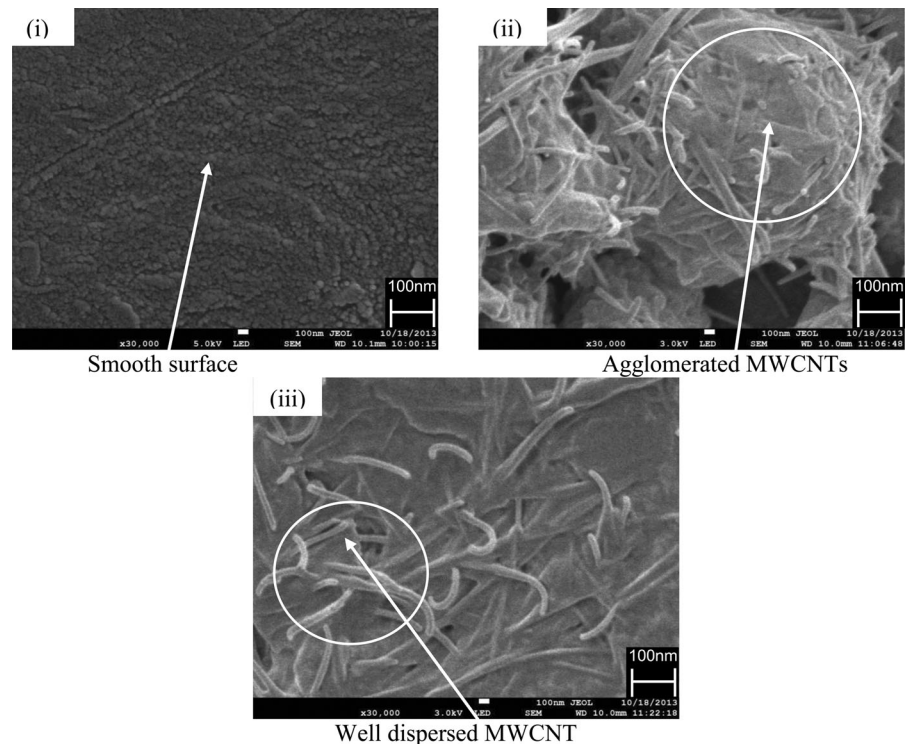


Fig. 1 Viscosity as a function of share rate for UPR, MWCNT-UPR, and THF-MWCNT-UPR

Fig. 2 FESM micrographs of non-fractured surface of **i** UPR, **ii** MWCNT–UPR, and **iii** THF–MWCNT–UPR



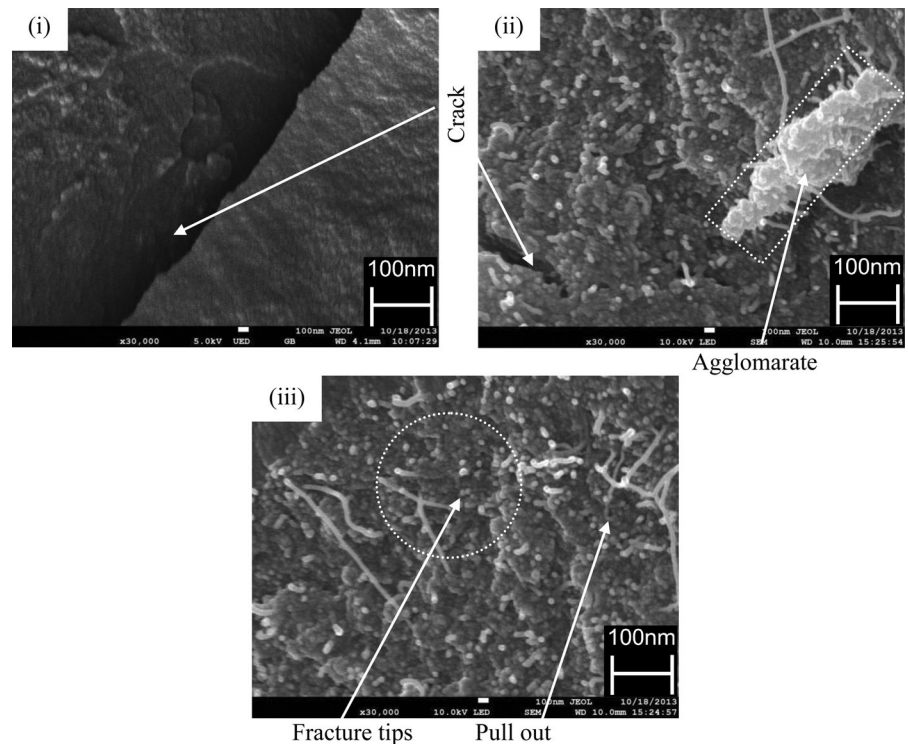
nanocomposite suspensions, with shear thinning behavior at low rate. Obviously, the shear viscosity of nanocomposites decreases with the increasing shear rate. The low shear rate up to 0.6 s^{-1} is useful to differentiate the viscosity difference of neat resin and other suspensions. Both composites' suspensions demonstrate higher viscosities than the neat resin at low shear rate. The THF–MWCNT–UPR reveals a greater viscosity than MWCNT–UPR at low shear rate, and the corresponding viscosities are 43,491 and 36,892 mPa s, which circuitously indicate a good MWCNT-dispersed system or a well compatibility between resin and nanotubes. Similar results have been observed for carbon-based nanoparticles dispersed in polyester resins, where the authors claimed a homogeneous dispersion of nanoparticles (Kim et al. 2006). The higher viscosity of THF–MWCNT–UPR than MWCNT–UPR at low shear rate may indicate stronger interfacial interactions among MWCNT and UPR molecules as well as the formation of percolated structure by the carbon nanotubes. It is reported that this structure breaks down as the shear rate increases, resulting in increase viscosities that are similar at high shear rates for all systems (Mohamed Abdalla et al. 2007). From these results, it is suggested that

MWCNT is well dispersed in THF solution, and when this suspension is introduced in UPR to produce THF–MWCNT–UPR, its UPR molecules are likely to wrap MWCNTs through uniform distribution and prevent them from agglomeration, which usually occurs in the sample MWCNT–UPR.

Surface morphology

Figure 2 illustrates FESEM micrographs of non-fractured surfaces of (i) UPR, (ii) MWCNT–UPR, and (iii) THF–MWCNT–UPR. The surface of UPR is comparatively smooth and consists of a plenty of nano-size lumps along with small cracks. The surface of MWCNT–UPR contains irregularly dispersed MWCNTs in UPR matrix with larger openings or voids and that of THF–MWCNT–UPR comprises homogeneously dispersed MWCNTs in UPR matrix showing no gaps. Agglomeration and homogeneous dispersion are indicated by circles. The surface of THF–MWCNT–UPR shows quite well dispersion of nanotubes, whereas aggregates of MWCNTs are observable in the surface of MWCNT–UPR. In case of the latter, some local submicron-size agglomerates exist. The Van der Waals force among the MWCNTs is basically responsible to

Fig. 3 Fractured surface morphologies of **i** UPR, **ii** MWCNT–UPR, and **iii** THF–MWCNT–UPR



make the clusters of nanotubes in the matrix of MWCNT–UPR, resulting in a poor wetting of them. In contrast, THF–MWCNT–UPR surface exhibits individual nanotubes being separated and embedded in the polymer matrix. These results strongly suggest that by means of solvent mixing, the MWCNTs are to some extent homogeneously dispersed in UPR matrix, indicating a good distribution of the nanotubes. The most striking observation found for nanocomposites is that huge cracks are not developed in the polymer–filler system, and the MWCNTs are stick to the polymer surface. The dispersion of MWCNTs seen in the micrographs are thus in agreement with the results of good wettability, as also detected by viscosity measurements.

The fracture morphologies of (i) UPR, (ii) MWCNT–UPR, and (iii) THF–MWCNT–UPR are displayed in Fig. 3. Cracks and agglomeration have been marked by arrows and a dotted rectangle. A large fracture is found on the surface of UPR, whereas small crack propagation regions and agglomeration are noticed on the surface of MWCNT–UPR. No visible fractures are seen in the matrix of THF–MWCNT–UPR. Several bright tips of MWCNTs remain in the matrix, and some of the nanotubes are traced to be

pulled out during stretching. These results also support a better adhesion between MWCNTs and UPR molecules. Thus, the THF solvent along with sonication reveals a good avenue of making fine dispersion of MWCNTs in resin matrix. Not only that but also the increased interfacial area of nanotubes in composites can lead to the change of segmental morphology and influence the mechanical properties of nanocomposite, as reported elsewhere (Kim et al. 2006; Desai and Haque 2005).

XRD structural analysis

Figure 4 represents the XRD profiles of different samples. The MWCNTs contain a broad peak at the scattering angle of $2\theta = 26.1^\circ$, which can be indexed by (002) planes of the graphitized MWCNTs (Wang et al. 2005). Another peak for MWCNTs seems to appear at lower angle less than $2\theta = 3^\circ$, which is probably the small angle scattering from all nanotubes or bundles of nanotubes adhered each to other, revealing information on the average size and distribution of MWCNTs in the UPR matrix.

On the other hand, polyester resin shows a broad peak at $2\theta = 20.2^\circ$ that corresponds to its partial

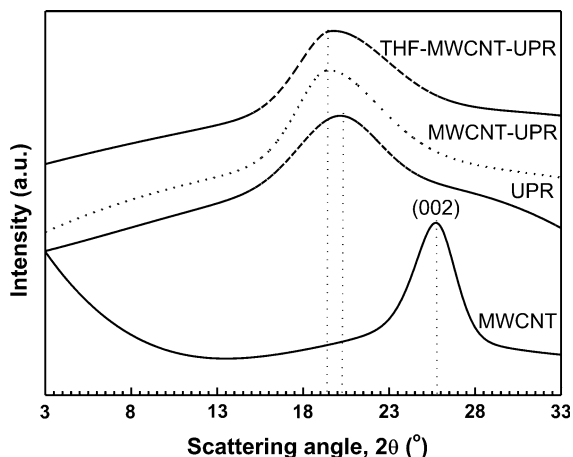


Fig. 4 XRD patterns of MWCNTs, UPR, MWCNT-UPR, and THF-MWCNT-UPR

crystalline and high amorphous natures, because the shape of the peak is neither so diffused as that shown by an amorphous sample nor so sharp as that revealed by a crystal. The average lattice spacing estimated from the peak is about 4.39 Å. When 0.5 wt% MWCNTs is introduced in UPR, the peak position is shifted to a lower scattering angle of 19.6°, which reveals a lattice constant of 4.53 Å. This increase in lattice parameter may be attributed to the intercalation of nanoparticles into the matrix, providing a lattice distortion in UPR crystals. From these results, it can be inferred that the MWCNTs are distributed well in resin matrix, leading to an increase in the interfacial adhesion among filler and matrix, which is consistent with the previously reported result for carbon black reinforced epoxy/resin (Abdel-Aal et al. 2008). Moreover, a slight decrease in peak width and increase in peak intensity for nanocomposites is also observed. The estimated degrees of crystallinity, χ_c , for virgin UPR, MWCNT-UPR, and THF-MWCNT-UPR are 14, 17, and 21 %, respectively. The observed decrease in peak width indicates that the size of the UPR crystallite increases and more population of UPR molecules take part in crystallization due to the presence of MWCNTs.

FTIR analysis

The FTIR spectra of MWCNT, UPR, MWCNT-UPR, and THF-MWCNT-UPR are demonstrated in Fig. 5. The spectrum of MWCNTs has been characterized in

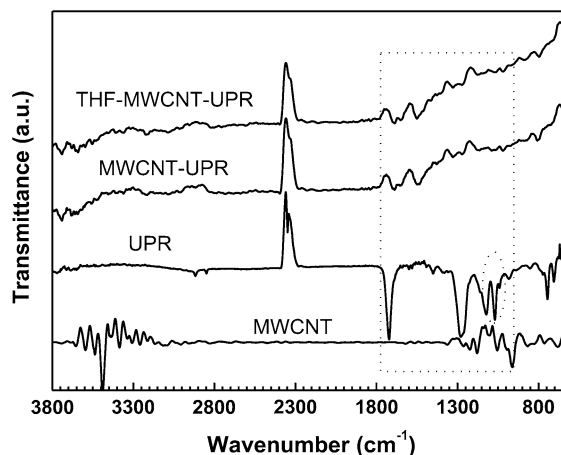


Fig. 5 FTIR spectra of different samples

details elsewhere (Stobinski et al. 2010). The appearance of a peak near 3,190 cm^{-1} shows the presence of various hydroxyl moieties on the carbon surface. There are some peaks in the range of 1,300–950 cm^{-1} , which may be due to the presence of some oxygen- and hydrogen-based groups as well as amorphous hydrocarbons in the supplied MWCNT, whose structural information may also exist in the spectrum. On the other hand, in the spectrum of UPR, two absorption bands, as mentioned by dotted circle, appear at 1,145 and 1,075 cm^{-1} of which the latter is attributed to C–O stretching vibrations (Mohamed Abdalla et al. 2007). The peaks that appear at 1,286 cm^{-1} may be assigned to CH_2 twisting, 1,381 cm^{-1} to CH_3 symmetrical bending, 1,640 cm^{-1} to aromatic ring stretching, and 1,728 cm^{-1} to C=O stretching vibrations. The bands in the range of 2,900–3,100 cm^{-1} correspond to stretching vibrations of C–H groups, such as CH_2 and CH_3 . The ester bonds (C–O–C) usually appear at 1,250 cm^{-1} , which is seemingly overlapped with the intense peak at 1,265 cm^{-1} . These results prove that UPR molecules bind together through chemical bond, especially ester bond.

Upon crosslinking between UPR molecules and interaction with MWCNTs, the most significant changes occur in the range of 1,800–950 cm^{-1} , as shown by dotted rectangle. Of these, the bands in the range of 1,700–1,200 cm^{-1} are usually assigned to vibrations of C=O, C–O, C–O–C, and C=C bonds in different environments (carboxylic acid, aromatic and unsaturated structural bonds, etc.). It is observed that the carbonyl (C=O) stretching band of UPR at

1,724 cm^{-1} has been shifted to a lower frequency of 1,699 cm^{-1} for MWCNT–UPR and 1,691 cm^{-1} for THF–MWCNT–UPR. This shift is perhaps due to the noticeable interaction between CNT and UPR through the electron cloud of ester groups and MWCNTs. Moreover, hydrogen bond formation between MWCNTs and UPR is evident, because the OH stretching frequency at 3,477 cm^{-1} for UPR is shifted to the low-frequency side: to 3,456 cm^{-1} for MWCNT–UPR and 3,454 cm^{-1} for THF–MWCNT–UPR. Probable bondings among MWCNTs and UPR molecules are represented by the Schemes 1 and 2 as shown in Fig. 6 in which Scheme 1 indicates the crosslinking between UPR molecules, and Scheme 2 shows that between MWCNT and UPR molecule.

Mechanical properties

Figure 7 exemplifies the stress–strain variations of the samples, showing the typical stress–strain curves that contain (i) toe, (ii) elastic, (iii) plastic, and (iv) fracture regions (Julkunen et al. 2009). The results indicate that both the values of breaking stress and breaking strain for nanocomposites are higher than those for UPR. Thus, the presence of MWCNTs in UPR not only enhances the mechanical strength but also makes the plastic deformation easy in the nanocomposites.

The plots for TS, TM, IS, and EB for different samples are shown in Fig. 8a and b. The values of TS, TM, IS, and EB % for UPR are 28.72 MPa, 1.247 GPa, 3.58 KJ/m^2 , and 4.6 %, and those for MWCNT–UPR are 31.51 MPa, 1.397 GPa, 4 KJ/m^2 , and 6.12 %, respectively. Thus, the TS, TM, IS, and EB % increase by an amount of 9.7, 12, 17, and 33 % after loading MWCNTs, respectively. On the other hand, the TS, TM, IS, and EB % values of THF–MWCNT–UPR are 35.13 MPa, 1.5 GPa, 4.6 KJ/m^2 , and 8.63 %, respectively. Therefore, the increases in TS, TM, IS, and EB % of THF–MWCNT–UPR from neat resin are 22.30, 20.30, 28.50, and 87.60 %, respectively. These results clearly demonstrate a good reinforcement effect of a small amount of MWCNTs on mechanical properties of the nanocomposites. The increases in TS, TM, IS, and EB % of THF–MWCNT–UPR from MWCNT–UPR are 11.5, 7, 9, and 41 %, respectively.

The increases in mechanical properties of THF–MWCNT–UPR are the results of solvent dispersion of MWCNTs and their good adhesion in the matrix,

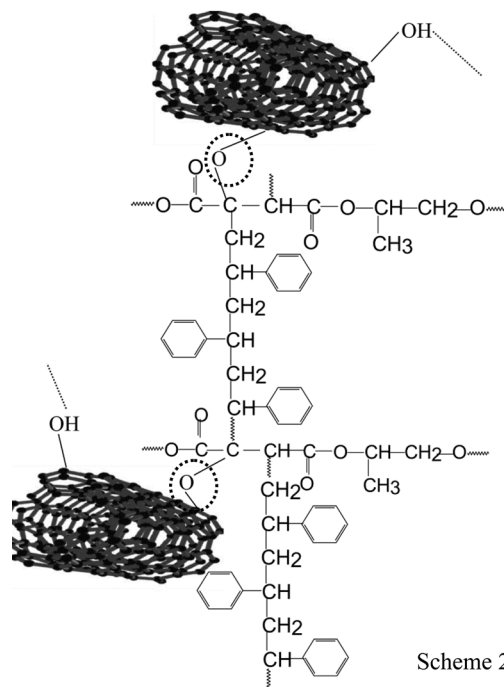
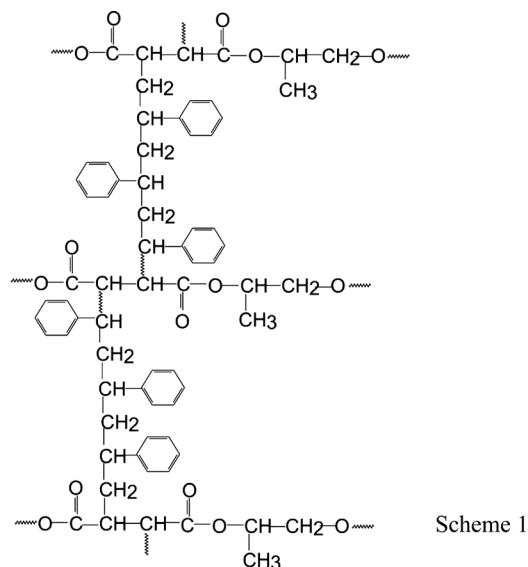


Fig. 6 Schematics for crosslinking between UPR molecules (Scheme 1) and between MWCNT and UPR molecule (Scheme 2)

which can be explicable using the following Neilson model (Nielson 1974):

$$A_Q = \frac{1}{(1 - \phi^{\frac{2}{3}})} \cdot \frac{TS_{\text{nanocomp}}}{TS_{\text{upr}}}, \quad (2)$$

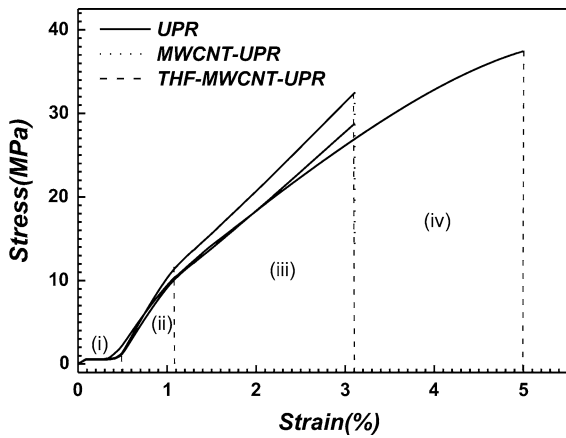


Fig. 7 The typical stress–strain curves of different samples

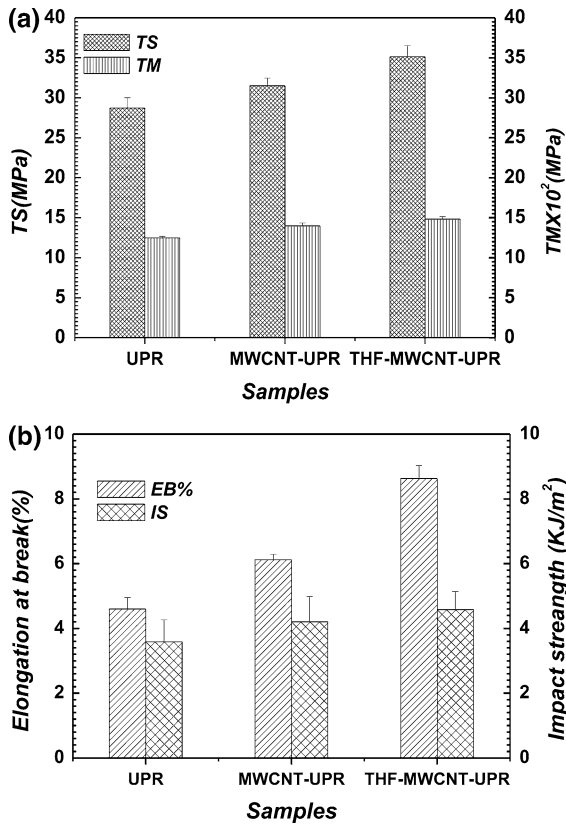


Fig. 8 The values of a TS and TM, as well as b EB % and IS of different samples

where A_Q accounts for the adhesion quality between polymer–filler interface; $TS_{nanocomp}$ and TS_{UPR} denote the tensile strength of the nanocomposite and the resin matrix, respectively; and φ represents the weight

fraction of the nanofiller. The calculated values of A_Q are 2.96 for MWCNT–UPR and 3.30 for THF–MWCNT–UPR. The improved mechanical properties of the THF–MWCNT–UPR over MWCNT–UPR and UPR are not only due to the good dispersion and adhesion of MWCNTs in the resin matrix as demonstrated by viscosity and FESEM, but also to the chemical bond formation between MWCNTs and UPR molecule, as verified by FTIR. A minor effect of crystallization in UPR in the presence of the nano-nucleating agent also renders the improving mechanical performances. When the dispersion has been made in the absence of THF, the MWCNTs undergo partial agglomeration, which limits the efficiency of reinforcement. Such a phenomenon was disclosed in other report (Wang et al. 2012). Clearly, agglomeration of MWCNTs narrows their active interfacial area and restricts their performance. In the present study, sonication in the presence of THF reduces the MWCNTs agglomeration. Indeed, the extraction of individual nanotube from MWCNTs bundles paves the way of affording both large surface area and strong interfacial interactions between the polymer and nanofiller interface, as declared elsewhere (Wang et al. 2012). These inherent advantages lead to efficient stress transfer between the MWCNTs and the UPR, thereby giving rise to enhanced mechanical performances. Moreover, higher elongations of nanocomposites indicate that MWCNTs are complimentary to more plastic deformation in the nanocomposites.

Thermal analysis

Figure 9 depicts the DSC thermograms of (i) MWCNTs, (ii) UPR (iii) MWCNT–UPR, and (iv) THF–MWCNT–UPR. The endothermic peak at the lower temperature region around 60–65 °C for all samples under investigation is ascribed to the glass transition temperature (T_g), allowing information of thermal translations of polymer chain molecules. Furthermore, the endothermic transition around 366–382 °C is related to the degradation temperature (T_d) of UPR. Instead of one endothermic peak as shown by UPR matrix, both nanocomposites exhibit a split melting endotherm into two peaks (T_{d1} and T_{d2}). The presence of double-degradation peaks for the nanocomposites may indicate the bond formation

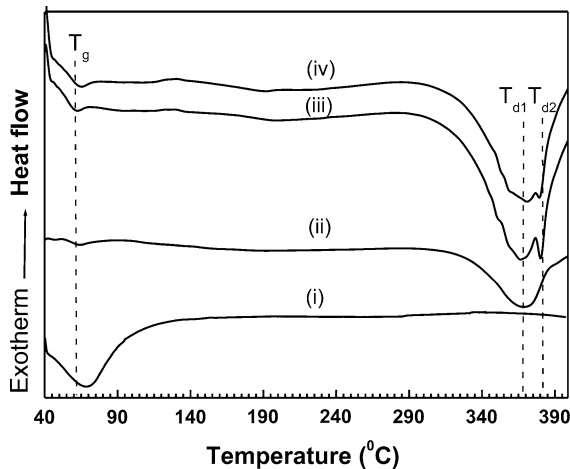


Fig. 9 DSC thermograms of **i** MWCNTs, **ii** UPR, **iii** MWCNT-UPR, and **iv** THF-MWCNT-UPR

between MWCNT and UPR. The sharp peak at T_{d2} is a precursor to identify the binding energy among nanotubes and UPR molecules. The calculated decomposition enthalpies ΔH per gm for UPR, MWCNTs-UPR, and THF-MWCNTs-UPR are 0.56, 0.64, and 0.81 J, which indicate the bond formation between UPR molecules and MWCNTs. Since ΔH per gm for UPR and MWCNTs-UPR is smaller than ΔH per gm for THF-MWCNTs-UPR, the number of bonds in the later on is greater, possibly because of the well-dispersed nanotubes. From the appearance of T_{d2} peak and in accordance with the results of FTIR, the formation of ester bond between MWCNT and UPR molecule is assumed to be developed, as shown in Scheme 2.

Evidently, the T_g value is slightly affected as much as the samples are concerned, and this trivial influence can be explained by the plasticization effect in the presence of nanofillers or lower degree of curing as well as inhomogeneous dispersion of MWCNTs. THF-MWCNT-UPR leads to the highest value of T_g among the samples investigated. Due to well dispersion of MWCNTs in THF-MWCNT-UPR, the nanocrystalline regions in matrix relatively become well-ordered as well as enhance the degree of curing, which restrict the resin chain mobility in the surrounding area of MWCNTs (Allaoui and El Bounia 2009; Seymour and Cooper 1973). Taking into account of the partial crystallinity in UPR matrix, some nucleating effect provided by the dispersed MWCNTs is to be

considered. The diffused XRD peaks of UPR, after MWCNTs inclusion, confirm the increase in crystallinity behavior of its matrix. In the presence of MWCNT nanofillers, a localized crystallization within nano-range takes place in the host matrix. Such a crystallization and enhancement in crystallinity in UPR by introducing carbon black have been enunciated in a very recently published article (Alam et al. 2014). Interestingly, while THF is used, a better dispersion of MWCNTs occurs in the nanocomposites. This in effect reduces the nucleation size to an individual MWCNT from their bundles or agglomerations.

TGA and DTG curves of UPR, MWCNT-UPR, and THF-MWCNT-UPR are demonstrated in Fig. 10. A multi-stage decomposition behavior of the materials is reflected in the results. The decomposition stages are, for example, (i) the release of

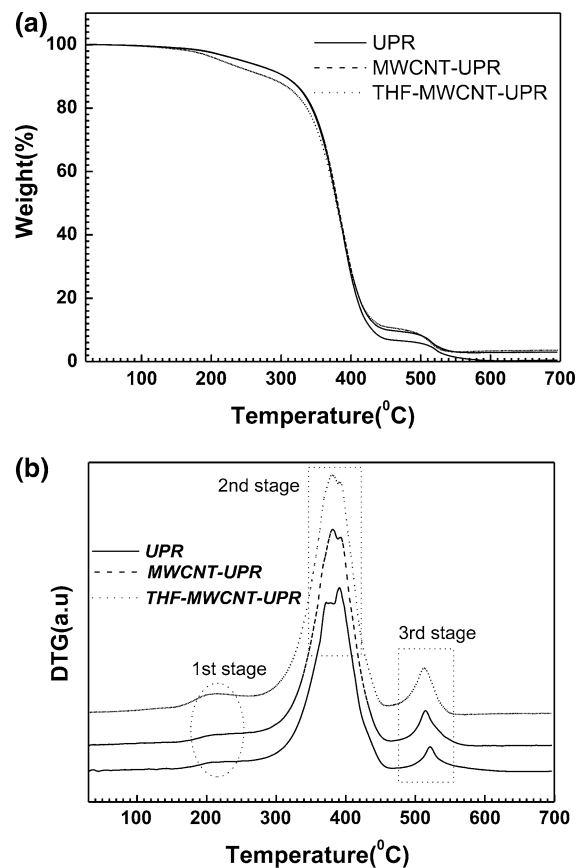


Fig. 10 The thermograms of **a** TGA and **b** DTG for various samples

volatile components, (ii) absorbed water (if any) from sample, (iii) the “onset” of degradation of molecules in the sample, and (iv) the presence of residual char (Moshiul Alam et al. 2012). In this study, thermal degradation of UPR takes place in four steps in which the onset of weight loss takes place at about 313 °C and finishes at 446 °C. On the other hand, this degradation in composites starts at relatively higher temperature than that found in neat resin. The TGA traces of both resin and nanocomposites seem to fall at 150 °C, indicating the emission of volatile components such as unreacted styrene, residual solvents, and uncross-linked polyester resin (Xia Cao and Lee 2003; Troitzsch 1990). Moreover, the TGA sharp-fall, which occurs at 331 °C for MWCNT–UPR and THF–MWCNT–UPR composites, looks different from the UPR, showing a three-step process in the temperature ranges of 299–425, 425–489, and 489–542 °C. These may be connected to the decomposition behavior of cross-linked resin composites. The degradation of cross-linked resin has been ascribed by the dissociation of C–C chain bonds and release of styrene at the site of dissociation (Mohamed Abdalla et al. 2007; Manfredi et al. 2006).

The peaks for various degradations in the samples are obtained from the DTG curves, as shown in Fig. 10b. Broad first-stage degradation occurs in all samples at 205 °C. At this temperature, the primary decomposition products were unreacted styrene and polyester resin (Mohamed Abdalla et al. 2007). The second-stage decomposition is seen in the range of 300–450 °C through split peaks at 380 °C for the samples. In this temperature region, the decompositions for MWCNT–UPR and THF–MWCNT–UPR are dissimilar to that for UPR. This is probably due to the bond formation between MWCNT and UPR, as revealed by FTIR. The corresponding decomposition temperature for nanocomposites is evaluated to increase by about 10 °C. This fact is suggested to be due to either by the bond formation or by the barrier effect of rigid MWCNTs, which strictly hindrance the thermal motion of the cross-linked chain segments in composites. However, the T_d values obtained by two measurements such as DSC and TGA are in close agreement. The residue content at 600 °C shows a significant difference between the UPR and nanocomposites, perhaps due to the MWCNT loading in resin (Abdel-Aal et al. 2008).

Conclusions

Among three different samples, such as UPR, MWCNT–UPR, and THF–MWCNT–UPR, the latter two were prepared by loading nanofiller through non-solvent and solvent dispersion with sonication methods, respectively. The dispersion and interaction of MWCNTs and matrix have been investigated by means of viscosity analysis, FTIR spectroscopy, and FESEM observation. The nano-suspension of THF–MWCNT–UPR exhibits the highest viscosity as compared to MWCNT–UPR and UPR at lower shear rate. The FTIR spectra of THF–MWCNT–UPR have provided evidence of more covalent interaction (ester bond) among UPR molecules and MWCNTs than MWCNT–UPR. The THF–MWCNT–UPR shows mechanical properties superior to other samples, due to well dispersion of MWCNT in matrix by solvent method. The FESEM analysis has confirmed an increased interaction between UPR and MWCNTs. The partial crystalline structure of UPR has been revealed by XRD, which shows more crystallinity in nanocomposites than UPR. DSC and TGA analyses exhibit covalent bond formation and an increased thermal degradation temperature for THF–MWCNT–UPR as compared to other two samples. In this work, almost homogeneous dispersion of CNTs in UPR matrix is achieved by THF solvent.

Acknowledgments Authors would like to acknowledge University Malaysia Pahang, Malaysia for providing financial support through the project RDU140319.

References

- Abdalla M, Dean D, Adibempe D, Nyairo E, Robinson P, Thompson G (2007) The effect of interfacial chemistry on molecular mobility and morphology of multiwalled carbon nanotubes epoxy nanocomposite. *Polymer* 48:5662–5670
- Abdel-Aal N, El-Tantawy F, Al-Hajry A, Bououdina M (2008) Epoxy resin/plasticized carbon black composites. Part II. Correlation among network structure and mechanical properties. *Polym Compos* 29(7):804–808
- Alam AKMM, Shubhra QTH, Islam MR, Barai Sanjoy, Mahabub (2011) Preparation and characterization of natural silk fiber reinforced polypropylene and synthetic e-glass fiber reinforced polypropylene composites: a comparative study. *J Compos Mater* 45(22):2301–2308
- Alam MK, Islam MT, Mina MF, Gafur MA (2014) Structural, mechanical, thermal and electrical properties of carbon black reinforced polyester resin composites. *J Appl Polym Sci*. doi:10.1002/app.40421

- Albdiry MT, Yousif BF (2013) Morphological structures and tribological performance of unsaturated polyester based untreated/silane-treated halloysite nanotubes. *Mater Des* 48:68–76
- Allaoui A, El Bounia N (2009) How carbon nanotubes affect the cure kinetics and glass transition temperature of their epoxy composites?—a review. *Express Polym Lett* 3(9):588–594
- Ausman KD, Piner Richard, Lourie Oleg, Ruoff RS (2000) Organic solvent dispersions of single-walled carbon nanotubes: toward solutions of pristine nanotubes. *J Phys Chem B* 104(38):8911–8915
- Barber AH, Cohen SR, Wagner HD (2003) Measurement of carbon nanotube-polymer interfacial strength. *Appl Phys Lett* 82:4140–4142
- Battisti A, Skordos AA, Partridge IK (2009) Monitoring dispersion of carbon nanotubes in a thermosetting polyester resin. *Compos Sci Technol* 69(10):1516–1520
- Breton Y, D'esarmot G, Salvétat JP (2004) Mechanical properties of multiwall carbon nanotube/epoxy composite: influence of network morphology. *Carbon* 42:1027–1030
- Desai AV, Haque MA (2005) Mechanics of the interface for carbon nanotube-polymer composites. *Thin-Walled Struct* 43:1787–1803
- Genhua Z, Wu J, Wang W, Pan C (2004) Characterizations of expanded graphite/polymer composites prepared by in situ polymerization. *Carbon* 42(14):2839–2847
- Gkikas G, Barkoula NM, Paipetis AS (2012) Effect of dispersion conditions on the thermo-mechanical and toughness properties of multi walled carbon nanotubes-reinforced epoxy. *Compos Part B* 43:2697–2705
- Gojny FH, Wichmann MHG, Köpke U, Fiedler B, Schulte K (2004) Carbon nanotube reinforced epoxy-composites: enhanced stiffness and fracture toughness at low nanotube content. *Compos Sci Technol* 64:2363–2371
- Gojny FH, Wichmann MHG, Fiedler B, Schulte K (2005) Influence of different carbon nanotubes on the mechanical properties of epoxy matrix composites—a comparative study. *Compos Sci Technol* 65:2300–2313
- Hemmati M, Rahimi GH, Kaganj AB, Sepehri S, Rashidi AM (2008) Rheological and mechanical characterization of multi-walled carbon nanotubes/polypropylene nanocomposites. *J Macromol Sci Part B* 47:1176–1187
- Julkunen P, Wilson W, Jurvelin JS, Korhonen RK (2009) Composition of the pericellular matrix modulates the deformation behaviour of chondrocytes in articular cartilage under static loading. *Med Biol Eng Comput* 47:1281–1290
- Kayatin MJ, Davis VA (2009) Visco-elasticity and shear stability of single-walled carbon nanotube/unsaturated polyester resin dispersions. *Macromolecules* 42:6624–6632
- Kim JA, Seong DG, Kang TJ, Youn JR (2006) Effects of surface modification on rheological and mechanical properties of CNT/epoxy composites. *Carbon* 44(10):1898–1905
- Kim M-G, Moon J-B, Kim C-G (2012) Effect of CNT functionalization on crack resistance of a carbon/epoxy composite at a cryogenic temperature. *Compos Part A* 43:1620–1627
- Kosar V, Gomzi Z (2010) Crosslinking of an unsaturated polyester resin in the mould: modelling and heat transfer studies. *Appl Math Model* 34:1586–1596
- Kota AK, Cipriano BH, Duesterberg MK, Gershon AL, Powell D, Raghavan SR, Bruck HA (2007) Electrical and rheological percolation in polystyrene/MWCNT composites. *Macromolecules* 40(20):7400–7406
- Kubota H (1975) Curing of highly reactive polyester resin under pressure: kinetic studies by differential scanning calorimetry. *J Appl Polym Sci* 19:2279–2297
- Li Quanxiang, Church Jeffrey S, Kafi Abdullah, Naebe Minoo, Fox Bronwyn L (2014) An improved understanding of the dispersion of multi-walled carbon nanotubes in non-aqueous solvents. *J Nanopart Res* 16:2513. doi:10.1007/s11051-014-2513-0
- Logakis E, Pandis C, Pissis P, Pionteck J, Pötschke P (2011) Highly conducting poly(methyl methacrylate)/carbon nanotubes composites: investigation on their thermal, mechanical, electrical and dielectric properties. *Compos Sci Technol* 71:854–862
- Lu KL, Lago RM, Chen YK, Green MLH, Harris PJF, Tsang SC (1996) Mechanical damage of carbon nanotubes by ultrasound. *Carbon* 34(6):814–816
- Manfredi LB, Exequiel S, Rodríguez, Wladyka-Przybylak M, Vazquez A (2006) Thermal degradation and fire resistance of unsaturated polyester, modified acrylic resins and their composites with natural fibres. *Polym Degrad Stab* 91:255–261
- Mina MF, Haque MA, Hassan Bhuiyan MK, Gafur MA, Tamba Y, Asano T (2010) Structural, mechanical and thermal studies of double-molded isotactic polypropylene nanocomposites with multi-walled carbon nanotubes. *J Appl Polym Sci* 118(11):312–319
- Mina MF, Shorowardy HS, Khan MA, Alam AKMM, Beg MDH (2013) Improved mechanical performances of triple super phosphate treated jute-fabric reinforced polypropylene composites irradiated by gamma rays. *J Appl Polym Sci* 130(1):470–478
- Mina MF, Beg MDH, Islam MR, Nizam A, Alam AKMM, Yunus RM (2014) Structures and properties of injection molded biodegradable poly(lactic acid) nanocomposites prepared with untreated and treated multi-walled carbon nanotubes. *Polym Eng Sci* 54(2):317–326
- Monti M, Puglia D, Natali M, Torre L, Kenny JM (2011) Effect of carbon nanofibers on the cure kinetics of unsaturated polyester resin: thermal and chemorheological modelling. *Compos Sci Technol* 71:1507–1516
- Moshiul Alam AKM, Beg MDH, Reddy Prasad DM, Khan MR, Mina MF (2012) Structures and performances of simultaneous ultrasound and alkali treated oil palm empty fruit bunch fiber reinforced poly(lactic acid) composites. *Compos Part A* 43:1921–1929
- Mukhopadhyay K, Dwivedi CD, Mathur GN (2002) Conversion of carbon nanotubes to carbon nanofibers by sonication. *Carbon* 40(8):1373–1376
- Nielson R (1974) Mechanical properties of polymers and composites. Marcel Dekker, New York
- Pavlidou S, Papispyrides CD (2008) A review on polymer-layered silicate nanocomposites. *Prog Polym Sci* 33:1119–1198
- Ritter U, Scharff P, Dmytrenko OP, Kulish NP, Prylutskyi YI, Grabovskiy YE, Belyi NM, Pinchuk TN, Alekseev AN, Sementsov YI, Gavrylyuk NA, Shlapatskaya VV (2010)

- Strength improvement of iPP/MWCNT nanocomposites. *Polym Compos* 31:179–184
- Seyhan AT, Gojny FH, Tanoglu M, Schulte K (2007) Critical aspects related to processing of carbon nano-tube/unsaturated thermoset polyester nanocomposites. *Eur Polym J* 43(2):374–379
- Seymour RW, Cooper SL (1973) Thermal analysis of polyurethane block polymers. *Macromolecules* 6(1):48–53
- Shubhra QTH, Alam AKMM (2011) Effect of gamma radiation on the mechanical properties of natural silk fiber and synthetic E-glass fiber reinforced polypropylene composites: a comparative study. *Radiat Phys Chem* 80:1228–1232
- Shubhra QTH, Alam AKMM, Quaiyyum MA (2011) Mechanical properties of polypropylene composites: a review. *J Thermoplast Compos Mater* 26(3):362–391
- Singh RP, Jain S, Ramarao P (2013) Surfactant-assisted dispersion of carbon nanotubes: mechanism of stabilization and biocompatibility of the surfactant. *J Nanopart Res* 15(10):1–19
- Stobinski L, Lesiak B, Kover L, Toth J, Biniak S, Trykowski G, Judek J (2010) Multiwall carbon nanotubes purification and oxidation by nitric acid studied by the FTIR and electron spectroscopy methods. *J Alloy Compd* 501:77–84
- Sun C-H, Yin L-C, Li F, Lu G-Q, Cheng H-M (2005) Van der Waals interactions between two parallel infinitely long single-walled nanotubes. *Chem Phys Lett* 403:343–346
- Troitzsch J (1990) *International plastics flammability handbook*. Hanser Publishers, New York
- Wang F, Arai S, Endo M (2005) The preparation of multi-walled carbon nanotubes with a Ni-P coating by an electroless deposition process. *Carbon* 43:1716–1721
- Wang J, Shi Z, Ge Y, Wang Y, Fan J, Yin J (2012) Functionalization of unzipped carbon nanotube via in situ polymerization for mechanical reinforcement of polymer. *J Mater Chem* 22:17663–17670
- Xia Cao L, Lee James (2003) Control of shrinkage and residual styrene of unsaturated polyester resins cured at low temperatures: I. Effect of curing agents. *Polymer* 44:1893–1902
- Zhang WL, Liu YD, Choi HJ (2011) Graphene oxide coated core-shell structured polystyrene microspheres and their electro rheological characteristics under applied electric field. *J Mater Chem* 21:6916–6921